Nano Res
DOI (automatically inserted by the publisher)
Review Article/Research Article **Please choose one**

Integrin Targeting with Peptide Bioconjugated to Semiconductor-Magnetic Nanocrystalline Heterostructures

Gianpiero Valente[1†], Nicoletta Depalo[2†], Ivan de Paola[3], Rosa Maria Iacobazzi[4], Nunzio Denora[4], Valentino Laquintana[4], Roberto Comparelli[2], Emiliano Altamura[1], Tiziana Latronico[5], Michele Altomare[2], Elisabetta Fanizza[1], Marinella Striccoli[2], Angela Agostiano[1,2], Michele Saviano[6], Annarita Del Gatto[3], Laura Zaccaro[3] (✉), and Maria Lucia Curri[2] (✉)

[1] Università degli Studi di Bari Aldo Moro, Dipartimento di Chimica, Via Orabona 4, 70125 - Bari, Italy
[2] Istituto per i Processi Chimico-Fisici-CNR UOS Bari, Via Orabona 4, 70125 - Bari, Italy,
[3] Istituto di Biostrutture e Bioimmagini-CNR, Via Mezzocannone, 16, 80134- Napoli, Italy.
[4] Università degli Studi di Bari Aldo Moro, Dipartimento di Farmacia – Scienze del Farmaco, Via Orabona 4, 70125 - Bari, Italy.
[5] Università degli Studi di Bari Aldo Moro, Dipartimento di Bioscienze, Biotecnologie e Biofarmaceutica, Via Orabona 4, 70125 - Bari, Italy.
[6] Istituto di Cristallografia-CNR, Via Amendola 122/O, 70126 Bari, Italy.
† These authors contributed equally.
Received: day month year / Revised: day month year / Accepted: day month year (automatically inserted by the publisher)

ABSTRACT

Binary asymmetric nanocrystals (BNCs), composed of a photoactive TiO_2 nanorod joined with a superparamagnetic γ-Fe_2O_3 spherical domain, have been embedded in polyethylene glycol modified phospholipid micelle and successfully bioconjugated to a suitably designed peptide containing RGD motif. The BNCs represent a relevant multifunctional nanomaterial, due to the coexistence in one particle of two distinct domains, characterized by high photoactivity and magnetic properties, respectively, particularly suited as phototherapy and hyperthermia agent as well as a magnetic probe in biological imaging. In order to targeting integrin expressed on activated endothelial cells and several types of cancer cells, RGD motif has been selected. The preparation of the RGD-peptide/BNC conjugates, comprehensively monitored by using complementary optical and structural techniques, has demonstrated a high stability and uniform dispersibility in biological media. The cytotoxicity of the RGD-peptide/BNC conjugates has been studied in vitro. The cellular uptake of RGD-peptide conjugates in the cells, assessed by means of two distinct approaches, namely confocal microscopy analysis and emission spectroscopy determination in cell lysates, has established the selectivity of the RGD-peptide-BNC conjugate for the $\alpha v\beta 3$ integrin, and, consequently, a high potential of the developed multifunctional nanomaterial for theranostic treatments of cancer.

KEYWORDS

Nanocrystalline Heterostructures, Photoactive semiconductor, Magnetic nanostructure, Multifunctional Nanosystem, Cyclic RGD Peptide, $\alpha v\beta 3$ Integrin, Bio-conjugation, Active Targeting

Address correspondence to Maria Lucia Curri, lucia.curri@ba.ipcf.cnr.it; Laura Zaccaro, lzaccaro@unina.it

1. INTRODUCTION

Multicomponent hybrid nanoparticles (NPs), consisting of two or more domains, are formed of materials with different composition, with high control over size, shape, and spatial orientation and with integrated multifunctionality. Such materials offer an enormous potential for biomedical applications, as they are able to combine multiple functions and tasks, as targeting and theranostic functions within a single nanoscale system, thus offering new and improved opportunities to overcome limitations associated with conventional diagnosis and therapy of several diseases, especially cancer [1-3]. Compared to more conventional chemotherapeutic agents or anti-angiogenic drugs, multifunctional colloidal NPs provide several advantages, including size, which allows them to passively accumulate at tumor site due to the enhanced permeability and retention (EPR) effect, and their ability to evade the immune system, and finally improving blood circulating half-life, thus lowering dosage [4]. In addition, the high surface to volume ratio of the NPs allows a high local density of targeting ligand conjugated at NP surface, and provide multiple and simultaneous interactions with cell surface, thus ensuring a very high active, powerful and still selective targeting of tumor or tumor-associated cells [5]. Among the synthetic ligands which can be conjugated to NP surface for an active targeting of tumor tissues, peptides present a number of advantages over a variety of different agents, including proteins, antibodies, folate, and carbohydrates, such as small size, easy preparation, functionalization and conjugation, low toxicity and immunogenicity, high affinity and specificity for the receptors. It is well documented that peptides containing the arginine-glycine-aspartate (RGD) sequence are able to bind to different kind of integrins, including $\alpha v\beta 3$, a membrane receptor overexpressed on both tumor and vasculature in many solid tumors, such as glioblastomas, melanomas, and ovarian, breast, and prostate cancers [6-8]. In this perspective, numerous linear and cyclic RGD peptides conjugated to NPs have been extensively investigated as candidate agents for tumor diagnosis, imaging, and therapy, using quantum dots, iron oxide NPs, gold nanospheres and nanorods, single and multi-walled carbon nanotubes [9-18].

In this work, binary asymmetric nanocrystals (BNCs) formed by a spherical γ-Fe_2O_3 magnetic domain epitaxially grown onto a lateral facet of a rod-like anatase TiO_2, have been incorporated into water dispersible micelles composed of polyethylene glycol modified phospholipids (PEG lipids) [19] and, for the first time, conjugated with a designed cyclic peptide containing the RGD motif.

The BNCs represent relevant multifunctional hybrid nanosystems characterized by a high level of structural complexity and compositional diversity, due to the coexistence in one particle of two distinct domains, that enable to combine synergistically the peculiar properties of both superparamagnetic γ-Fe_2O_3 NCs and photoactive TiO_2 nanorods (NRs) in a system particularly suited as phototherapy and hyperthermia agent, as well as, a magnetic probe in biological imaging. Superparamagnetic iron oxide NPs (SPIONs) have been extensively recognized as a very promising and safe class of materials for diagnosis and therapy of cancer. Their theranostic impact can be clearly envisaged as they can effectively improve contrasting features in magnetic resonance imaging (MRI), perform drug delivery and induce hyperthermia. Indeed, magnetic NPs exhibit not only a superior biocompatibility, but also a greater sensitivity in the micromolar or nanomolar range than other agents, such as gadolinium complexes, so they can be used as MRI contrast agents. In addition, specific targeting of magnetic NP can help also direct therapeutic agents to localized disease sites, thus reducing drug wastage, lowering the frequency of drug administration and avoiding unwanted side-effects in the regions surrounding the tumor [20, 21].

On the other hand, TiO_2 NPs, characterized by excellent photocatalytic activity, low toxicity and high chemical stability, are definitely among the promising inorganic photosensitizers for photodynamic therapy (PDT) against cancer [22, 23]. Under the irradiation of UV light, the photo-induced electrons and holes can react with hydroxyl ions or water to form powerful oxidative

radicals able to destroy the tumor cells. Moreover, TiO_2 NPs could be retained in the body for a time much longer than that of conventional organic photosensitizers. The limitation deriving from the need of UV irradiation for an effective treatment, can be overcome as UV light can be brought to the specific location of the cancer cells by means of an optical fiber; in addition several routes are under investigation in order to enhance the visible-light absorbance of TiO_2 NPs, by doping or combining them with metal or non-metal components (Pt, CdS, iron oxides) [24-26].

In this paper, BNCs have been synthesized by means of a colloidal chemistry approach that allows a high control over size, shape and composition. The further BNC encapsulation in the hydrophobic core of PEG-modified phospholipid micelles has resulted in their prompt dispersibility and high stability in aqueous medium, due to the steric hindrance of the PEG coating surface of the micelles. In addition PEG functionalization has been reported to bring an efficient anti-opsonization effect in physiological environment, inducing a significant inhibition of protein absorption and less recognition by macrophages [27].

Here, BNC/Micelles have been functionalized with a purposely designed peptide, characterized by i. a GK (glycine-lysine) motif for the covalent binding to the BNCs, ii. a dansyl group (DNS) as fluorescent marker, and iii. a cyclic RGD sequence able to promote a specific targeting for integrin recognition.

Each step of the work has been thoroughly monitored by means of optical, morphological and structural techniques, demonstrating that peptide/BNC conjugates, stable in aqueous solution long enough to perform *in vitro* experiments, can be achieved. Citotoxicity of the RGD peptide/BNC conjugates has been assessed by means of two in vitro models, namely human melanoma cells (WM266), which overexpress $\alpha v\beta 3$ integrin and human breast cancer cells (MCF-7) which express the integrin $\alpha v\beta 3$ at very low level. Finally, confocal microscopy investigation has further highlighted the uptake of RGD conjugates on WM266 cell line, establishing the selectivity of the RGD-peptide-BNC conjugate for the $\alpha v\beta 3$ integrin, and, consequently, a high potential of the multifunctional bioconjugated nanomaterial for theranostic applications.

2. EXPERIMENTAL

2.1. Materials

All chemicals were of the highest purity available and were used as received without any further purification or distillation. Titanium tetraisopropoxide ($Ti(OPri)_4$ or TTIP, 99.999%), trimethylamino- N-oxide dihydrate or anhydrous ($(CH_3)_3NO$ or TMAO, 98%), oleic acid ($C_{18}H_{33}CO_2H$ or OLEA, 90), 1-octadecene ($C_{18}H_{36}$ or ODE, 90%), oleyl amine ($C_{17}H_{33}NH_2$ or OLAM, 70%), iron pentacarbonyl ($Fe(CO)_5$, 98%), and dodecan-1,2-diol ($C_{12}H_{24}(OH)_2$ or DDIOL, 90%), phosphotungstic acid (99.995%), Triton X100 and Phalloidin-Tetramethylrhodamine B isothiocyanate (Phalloidin-TRIC) were purchased from Sigma-Aldrich. Reagent-grade salts for phosphate (PBS) and Tris(hydroxymethyl) aminomethane hydrochloride (Tris-HCl) buffer solutions were obtained from Sigma. 1,2-Dipalmitoyl-sn-glycero-3-phosphoethanolamine-N-[methoxy (poly(ethylene glycol))-2000] (16:0 PEG-2-PE) and, 1,2-distearoyl-snglycero-3-phosphoethanolamine-N-[carboxy(poly(ethylene glycol))-2000] (DSPE-PEG(2000)carboxylic acid) were purchased from Avanti Polar Lipids. 1-Ethyl-3-(3-dimethylaminopropyl) carbodiimide hydrochloride (EDC) and N-hydroxysulfosuccinimide (sulfo-NHS) were purchased from Pierce. DL-Mandelic acid (⩾99%), titanium ion standard solution (998 ± 4 mg/L, Ti^{4+} in H_2O), iron ion standard solution (1000 ± 4 mg/L, Fe^{2+} in H_2O), ammonium hydroxide solution (25%), perchloric acid (70%), nitric acid (>69.5%), hydroxylamine hydrochloride (⩾ 99.0%), 1,10-Phenanthroline (⩾99%), ammonium acetate (⩾ 98%), acetic acid (99.8%, anhydrous) and hydrochloric acid (37%) were purchased from Fluka. Acetonitrile (ACN) was purchased from Sigma-Aldrich (CromaSolv® gradient grade, purity ⩾99.9%). All solvents used were of analytical grade and purchased from Aldrich. All aqueous solutions were prepared by using water obtained from a Milli-Q gradient A-10 system (Millipore, 18.2 MΩ cm, organic carbon content⩾4 μg/L). Phenylsilane,

$Pd(PPh_3)_4$, hydrazine solution, dansyl chloride (DNS-Cl), N,N'-Diisopropylethylamine (DIPEA) and piperidine were purchased from Sigma-Aldrich. Polypropylene reaction vessels and sintered polyethylene frits were supplied by Alltech Italia. NovaSyn TGR resin, 2-(1H-benzotriazole-1-yl)-1,1,3,3-tetramethyluronium hexafluorophosphate (HBTU), 1-hydroxybenzotriazole (HOBT), benzotriazole-1-yl-oxytripyrrolidinophosphonium hexafluorophosphate (PyBop) and all amino acids were from Novabiochem. DMEM (Dulbecco's Modified Eagle Medium), RPMI 1640 (Roswell Park Memorial Institute - 1640) medium, FBS (Fetal Bovine Serum) penicillin (100 U/mL) and streptomycin (100 μg/mL) were purchased from Lonza.

2.2 Peptide Synthesis

The cyclic $RGD(GK)_2$-DNS and the linear $(GK)_2$-DNS peptides were manually synthesized using the fluorenylmethyloxycarbonyl (Fmoc) solid-phase strategy (0.1 mmol). The synthesis syntheses were carried out on NovaSyn TGR resin (loading 0.25 mmmol/g), using all standard amino acids except for Fmoc-Glu-OAll (N-α-Fmoc-L-glutamic acid α- allyl ester), Fmoc-Lys(ivDde)-OH (N-α-Fmoc-N-ε-1-(4,4-dimethyl-2,6-dioxocyclohex-1-ylidene) - 3-methylbutyl-L-lysine) and Fmoc-D-Phe-OH (N-α-Fmoc-D-phenylalanine). The amino acids in 10-fold excess were preactivated with HBTU (9.8 equiv)/ HOBT (9.8 equiv)/DIPEA (10 equiv) in DMF for 5 min and then added to the resin suspended in DMF. The reaction was carried out for 1h and the coupling efficiency was assessed by the Kaiser test. The Fmoc protecting group was removed by treatment with 30% piperidine in DMF (3 x 10 min). For $RGD(GK)_2$, before the final Fmoc deprotection of the Arg1, selective deprotection of the Glu residue from the allyl group was carried out by treatment of the peptidyl resin with $PhSiH_3$ (24 equiv)/$Pd(PPh_3)_4$ (0.25 equiv) in DCM (3 x 10 min). The cyclization reaction between αNH of D-Phe and αCO of Glu was carried out on the resin with PyBop (1.5 equiv)/HOBT (1.5 equiv)/DIPEA (2 equiv) in DMF for 3 h and monitored by the Kaiser test. To label $RGD(GK)_2$ and $(GK)_2$ with the DNS fluorophore, ivDde protecting group was removed from the ε-amino group of the lysine by treatment of the peptidyl resin with a solution of hydrazine 2% in DMF (3 min x 20). DNS labeling was performed with 2 equiv of DNS-Cl and 4 equiv of DIPEA in DMF for 5 h. The peptides were cleaved off the resin by treatment with a mixture of trifluoroacetic acid (TFA)/water/triisopropylsilane (95:2.5:2.5 v/v/v) for 3 h at room temperature. The resins were filtered, and the crude peptides were precipitated with diethyl ether, dissolved in a H_2O/ACN solution, and lyophilized. The products were purified by preparative RP-HPLC on a Shimadzu system equipped with a UV−visible detector SPD10A using a Phenomenex Jupiter Proteo column (21.2 ×250 mm; 4 μm; 90 Å) and a linear gradient of H_2O (0.1% TFA)/ ACN (0.1% TFA) from 5 to 70% of ACN (0.1%TFA) in 30 min at flow rate of 20 mL/min. The collected fractions containing the peptides were lyophilized. The identity and purity of the compounds were assessed by an AGILENT Q-TOF LC/MS instrument equipped with a diode array detector combined with a dual ESI source on a Agilent C18 column (2.1 x 50 mm; 1.8 μm; 300 Å) at a flow rate of 200 μL/min and a linear gradient of H_2O (0.1% TFA)/CHCN (0.1% TFA) from 5 to 70% of ACN (0.1% TFA) in 12 min.

2.3 Synthesis of BNCs

The BNC synthesis was carried out starting from pre-synthesized TiO_2 nanorods (NRs) [19, 28]. Briefly, TiO_2 NRs were synthesized by adding a mixture of 70 g of oleic acid (OLEA, dried at 110°C for 1 h) and 10 mmol of TTIP to an aqueous TMAO solution (2 M, 5 mL) at 100°C for 96 h. Subsequently, the TiO_2 NRs were separated from their growing mixture upon methanol addition and purified by repeated cycles of methanol addition/centrifugation. The BNCs were obtained by loading a TiO_2 NR stock solution (1 M, 0.5 mL) with ODE (20 mL), DDIOL (2.5 mmol), OLAM (3 mmol), and OLEA (3 mmol) into a three-necked flask connected to a reflux condenser and dried at 110 °C. The reaction mixture was left stirring for 1 h and then heated under N_2 flux to 250 °C. Subsequently, 1 mL of an $Fe(CO)_5$ solution (1 M), in previously degassed ODE, was quickly injected and the temperature was then lowered to 130 °C. Finally,

the reaction mixture was cooled to room temperature after exposure to air for 60 min. The BNCs were collected by adding a solution containing 2-propanol and acetone (1:1), collected via centrifugation and dispersed in chloroform [28].

2.4 Incorporation of the BNCs in PEG-Modified Phosholipid Micelles

140 μL of a BNC stock solution (0.08 M) were dissolved in chloroform (710 μL) with 120 μL of 16:0 PEG-2-PE ($3.5*10^{-2}$ M) and 30 μL of DSPE–PEG(2000)carboxylic acid ($3.5*10^{-2}$ M). A dried BNC/PEG-lipid layer was attained by chloroform evaporation under N_2 flux and then kept under vacuum for 1 h. Subsequently, 2 mL of PBS buffer (10 mM, pH 7.2) was added to the film. BNC/PEG-lipid micelles were repeatedly heated to 80°C (with periodic vigorous mixing) and subsequently cooled to room temperature (three cycles). After centrifugation (13700xg for 25 min), the supernatant was recovered and filtered by using 0.2 μm filters (Anotop, Whatman) [19]. Empty PEG lipid micelles were prepared following the same protocol, just without BNC addition.

2.5 One-Step Bioconjugation of the BNC/Micelles with $(GK)_2$-DNS Peptide

A BNC/micelle suspension (2 mL) in PBS buffer (10 mM, pH 7.2) was incubated with freshly prepared EDC (5 mM) and sulfo-NHS (12.5 mM) solutions for 15 min at room temperature. Subsequently the $(GK)_2$-DNS was added and the mixture was gently stirred for 2 h. After the addition of Tris-HCl buffer solution (30 mM), the peptide/BNC conjugates were recovered by ultracentrifugation (200000xg) for 16 h and were separated from unreacted cross-linker molecules, quenching agent, and free peptides. Another cycle of re-dispersion and re-precipitation with PBS buffer (2 mL) was performed to obtain a high level of purification.

2.6 Two-Step Bioconjugation of the BNC/Micelles with RGD$(GK)_2$-DNS peptide

Firstly, freshly prepared EDC (5 mM) and sulfo-NHS (12.5 mM) solutions were added to a BNC/micelle suspension (2 mL) in PBS buffer, resulting in a final concentration of 5 and 12.5 mM, respectively. The mixtures were incubated for 15 min at room temperature. The excess of linker was removed from the solution by ultracentrifugation (200000xg) for 2 h. The activated BNC/micelle pellet was re-suspended in PBS buffer (2 mL) and incubated with RGD$(GK)_2$-DNS peptide for 2 h. Tris-HCl buffer solution (30 mM) was added to quench the reaction and the peptide/BNC conjugates were centrifugated (200000xg) for 16 h and washed with PBS buffer. The supernatant was removed and the particle pellet was re-suspended in PBS buffer and stored at -20°C until used.

2.7 Determination of the Peptide Content of Peptide/BNC Conjugates

The peptide content of peptide/BNC conjugates was determined by creating of a calibration curve. In particular, measurements of the photoluminescence (PL) intensity were recorded as a function of peptide concentration ($(GK)_2$-DNS or RGD$(GK)_2$-DNS peptide) in a aqueous solution of BNC/micelles at the same concentration of the bioconjugate samples, being the PL emission properties of DNS group sensitive to the polarity of the local environment. Finally, the calibration curve was obtained by plotting the area under the curve of PL emission band in the wavelength range between 400 and 700 nm versus peptide concentration.

2.8 Acid Digestion of BNC/Micelles and Peptide/BNC Conjugates

1 mL of BNC/micelles or peptide/BNC conjugates, dispersed in PBS aqueous solution, were diluted by adding ultrapure water (2-3 mL) and nitric acid (0.5 mL). The mixture was cautiously heated reducing its volume, until the digestion was complete. After cooling, the residual sample was hydrated with ultrapure water (~1 mL). Subsequently, perchloric acid (0.5 mL) was added and the sample was allowed to dry by heating. Finally, the digested sample was reconstituted by adding hydrochloric acid (20 μL, pH 2-2.5) and ultrapure water until a volume of 50 mL.

2.9 Anodic Stripping Voltammetry

Each digested sample, obtained by acid attack, was analyzed to determine the Ti^{4+} ion concentration, by means of anodic stripping voltammetry on a

hanging dropping mercury electrode (HDME) using a Metrohm 757 VA Computrace voltammeter. 1 mL of DL-mandelic acid (0.4 M) was used as a background electrolyte, adjusting the pH value to 3 (ammonium hydroxide solution).

2.10 Colorimetric analysis

10 mL of sample, digested by acid attack, was diluted by adding ultrapure water (20 mL) and hydrochloric acid (2 mL, 37%), and heated to boiling point until complete solubilization. After cooling, 0.5 mL of hydroxylamine hydrochloride (100 g/L) was added to the mixture, promoting the complete reduction of ferric ions to ferrous ions. Subsequently 2 mL of 1,10-phenanthroline were introduced, adjusting the pH value to 3 (ammonium hydroxide solution). Finally, the mixture was diluted, under vigorous stirring, in order to achieve a final volume of 50 mL. The Fe^{2+} ion concentration in the sample was determined by colorimetric analysis using a Dr. Lange filter photometer LP 1 W.

2.11 Cell Culture

Human breast carcinoma MCF-7 and human melanoma WM266 cell lines were cultured in DMEM and RPMI 1640 nutrient, supplemented with 10% heat inactivated FBS, 2 mM L-glutamine, 100 U/ml penicillin and 100 μg/ml streptomycin. All cells were maintained in a humidified incubator containing 5% CO_2 at 37 °C.

2.12 Cytotoxicity Assays

Cytotoxicity of BNC containing micelles and peptide/BNC conjugates were determined by performing the 3-(4,5-dimethylthiazol-2-yl)-2,5-diphenyl-tetrazolium bromide (MTT) assay and expressed as IC50 values (50% growth inhibitory concentration). Cells were dispensed into 96-well μL plates at a density of 5.000 cells/well. Untreated cells were used as control. After incubation for 12 h, peptide/BNC conjugates ranging from $2.27*10^{-6}$ to 0.113 mg/mL (γ-Fe_2O_3 concentration) were added to each well. Subsequently, the plates were incubated at 37 °C for 72 h. An amount of 10 μL of 0.5% w/v MTT was further added to each well and the plates were incubated for additional 3h at 37 °C. Finally the cells were lysed by addition of DMSO/EtOH (1:1) mixture (100 μL). The absorbance at 570 nm was determined using a Perkin Elmer 2030 multilabel reader Victor TM X3.

2.13 Determination of peptide/BNC conjugate fluorescence in cell lysates

MCF-7 and WM266 cells were seeded in 60-mm dishes (500.000 cells per dish) and incubated for 12 h. Subsequently, cells were treated with peptide/BNC conjugates at a final γ-Fe_2O_3 concentration of $2.27*10^{-3}$ mg/mL in medium. After 12 h, medium was removed and cells were washed with PBS buffer (5 mL) and lysed in 500 μL lysis buffer (10 mM TRIS-HCl, 150 mM NaCl, 0.5% Triton-X-100, pH 7.5). A cell scraper was used to remove and lyse residual cells. Lysates were transferred to Eppendorf tubes and centrifugated (13700xg for 10 min) to remove cell debris. The same experimental procedure was used to recover lysates of untreated cells for the both cell lines. Subsequently, 500 μL of the supernatant were used to record the PL spectrum and finally, Bradford protein assay was performed by using 10 μL of cell lysate for each sample. The PL signals were corrected for the amount of the protein in the samples, in order to determine the mean PL intensity. The mean PL intensity of the lysates recovered by cells incubated with conjugate samples was also correct for the mean background PL of the lysates obtained from untreated cells.

2.14 Photophysical Characterization

Absorption and photoluminescence measurements were performed by means of a UV/vis/NIR Cary 5 spectrophotometer (Varian) and the Eclypse spectrofluorimeter (Varian), respectively. The optical measurements on the BNC solution were carried out at room temperature on the solution obtained directly from synthesis without any size-sorting treatments. BNC/micelles and peptide/BNC conjugates were investigated in PBS buffer at room temperature.

2.15 ATR-FTIR Spectroscopy

Mid-infrared spectra were acquired with a Perkin-Elmer Spectrum One FTIR spectrometer equipped with a deuterated tryglicine sulfate

(DTGS) detector. The spectral resolution used for all experiments was 4 cm^{-1}. For ATR measurements, the internal reflection element (IRE) used was a three-bounce 4-mm-diameter diamond microprism. Cast films were prepared directly on the internal reflection element by depositing the solution of interest (3-5 μL) onto the upper face of the diamond crystal and allowing the solvent to evaporate.

2.16 HPLC-UV-Fluorescence Analysis

HPLC-UV-Fluorescence investigation was performed by using a Varian Prostar system consisting of two 210 pumps with 5 mL/min heads, a 325 UV/Vis dual wavelength detector and a fluorescence detector. The flux was set to 1 mL/min, the injected volume was 20 μL and the column was a PhenomenexSynergi 4μm Hydro-RP 80A C-18 (25 x 0.46 cm, 4 micron) with the following gradient: 95% Milli-Q water and 5% ACN for 2 minutes and then from 95% Milli-Q water and 5% ACN to 100% ACN in 15 minutes.

2.17 Particle size, size distribution and surface charge

Hydrodynamic diameter (size), size distribution and colloidal stability of the micelles containing BNCs, before and after bioconjugation reaction with peptides, were detected using a Zetasizer Nano ZS, Malvern Instruments Ltd., Worcestershire, UK (DTS 5.00). In particular, size and size distribution were determined by means of dynamic light scattering (DLS) after sample dilution in demineralized water. Size distribution is described in terms of polydispersity index (PDI). The ζ-potential measurements, *i. e.* the surface charges, were carried out by using a laser doppler velocimetry (LDV) after sample dilution in KCl aqueous solution (1 mM). All reported data are presented as mean values ± standard deviation of three replicates.

2.18 Transmission Electron Microscopy

Transmission Electron Microscopy (TEM) analysis was performed by using a Jeol JEM-1011 microscope, working at an accelerating voltage of 100 kV. TEM images were acquired by a Olympus Quemesa Camera (11 Mpx). The samples were prepared by dropping on the 400 mesh amorphous carbon-coated Cu grid a BNC chloroform dispersion or, alternatively, a BNC/micelle or peptide/BNC conjugate aqueous solution, and letting the solvent to evaporate. For the positive staining TEM observation, after the sample deposition, the grid was dipped in a 2% (w/v) phosphotungstic acid solution for 30 seconds. Staining agent excess was removed from the grid by rinsing with ultrapure water (dipping the grid in ultrapure water three times for 10 seconds). The sample on the grid was left to dry over night and finally stored in a vacuum chamber until analysis. For the negative staining TEM investigation, 30 μL of a 2% (w/v) phosphotungstic acid solution were cast on the grid where the sample was previously deposited. Staining agent excess was removed by blotting, at the edge of the grid, with filter paper, wetted with ultrapure water. After complete drying of the sample, the grid was stored in a vacuum chamber until analysis. Size statistical analysis (NP average size and size distribution) of the samples was performed by means of freeware Image J analysis program. In particular the average NP size and the percentage relative standard deviation (σ%) were calculated for each sample, to define NP size distribution. At least 200 objects were counted for each investigated sample.

2.19 Confocal Microscopy

Laser scanning confocal microscopy was performed on a Leica TCS SP5-II (Leica Microsystems, Germany) confocal inverted microscope using a ×63, 1.40 numerical aperture oil immersion lens for imaging. Laser beams with 405 nm and 542 nm excitation wavelengths were used for Dansyl and Phalloidin-TRITC imaging, respectively. Confocal images for WM266 cells, which are about 6-μm thick, were acquired, by taking 12 z-stacks of typically 0.5 μm thick slices. Each confocal image was collected by three line average and two frame average to significantly increase signal to noise ratio. Single confocal sections, z-stack images, and image rendering of confocal data files were processed using LAS AF LITE software (Leica microsystems, Germany). Images were acquired on fixed cells, namely WM266 cells (105 cells/well) were grown on glass bottom dishes (WillCo-Dish®) for 24 h and then exposed to

BNC/Micelles/RGD$(GK)_2$-Dansyl peptide conjugate at γ-Fe_2O_3 concentration of 0.0227 mg/ml. Following the incubation period of 1h, 3 h and 24 h, cells were washed two times with PBS and then fixed for 10 min with 4% w/v paraformaldehyde in PBS buffer. After two washing cycles by using PBS buffer, cells were permealized with Triton X-100 0,1% for 5 min, and after two washes (PBS buffer), incubated for 1h at 37°C with 10µl/ml Phalloidin-TRITC (Sigma-Aldrich) used as F-actin markers. After the staining with the appropriate marker, cells were imaged.

3. RESULTS AND DISCUSSION

Hydrophobic asymmetric BNCs, consisting of a semiconductor TiO_2 NR joined to a magnetic γ-Fe_2O_3 spherical domain, have been synthesized by a seeded colloidal technique and encapsulated in PEG-terminated phospholipid micelles that ensure the BNC dispersibility and stability in aqueous solution. Subsequently, the BNC containing PEG lipid micelles have been conjugated with two different fluorescent peptides with increasing structural and functional complexity, namely RGD$(GK)_2$-DNS and $(GK)_2$-DNS (Fig. 1).

The $(GK)_2$-DNS peptide has been designed starting from $(GC)_2$ peptide, previously reported as an effective capping motif to functionalize gold nanoparticles [9]. In $(GK)_2$-peptide, the cysteine residues have been replaced with lysine, in order to allow the formation of covalent bonds with the carboxylic groups onto the PEG moieties of the BNC/micelle surface, and a DNS group as fluorescent probe has been introduced in the middle of the sequence (Fig. 1a).

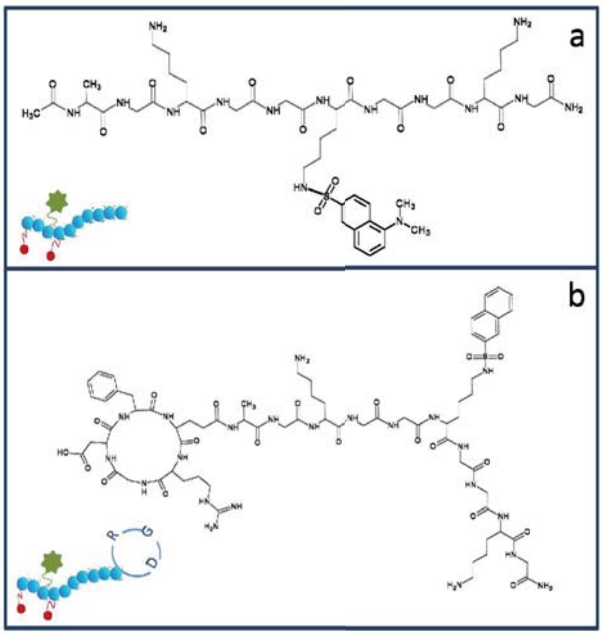

Figure 1 Peptide sequences of a) $(GK)_2$-DNS and b) RGD$(GK)_2$-DNS

The cyclic RGD sequence has been then added to the peptide framework, in order to achieve the integrin recognition, thus resulting in RGD$(GK)_2$-DNS peptide (Fig. 1 b).

The experimental conditions, such as reagent concentration and reaction time, for the bioconjugation process, have been set up preliminary investigating $(GK)_2$-DNS peptide, and obtaining $(GK)_2$-DNS-peptide /BNC/Micelle conjugates as useful control nanosystems to compare with RGD$(GK)_2$-DNS-peptide /BNC/Micelle conjugates in the further evaluation of the effect of the RGD sequence on the selective targeting.

A scheme depicting the steps leading to the BNC/micelles conjugation with RGD$(GK)_2$-DNS has been reported in Chart 1.

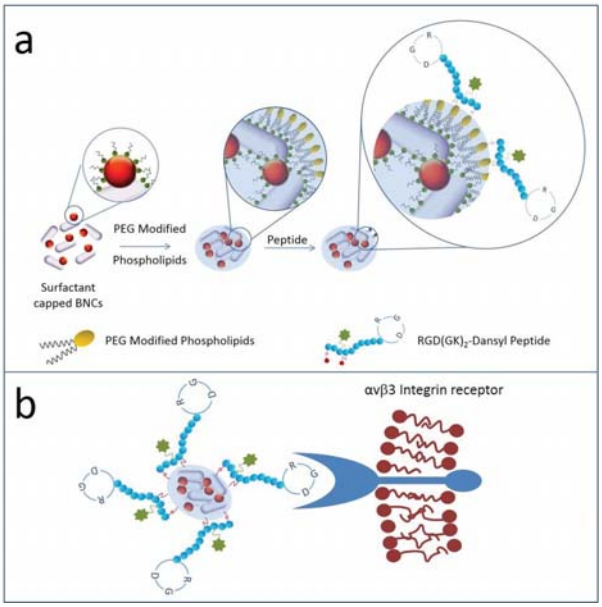

Chart 1 Schematic illustrations of a) BNC functionalization by PEG-modified phospholipids and conjugation to RGD(GK)$_2$-DNS peptide b) molecular recognition process between RGD(GK)$_2$-DNS-peptide/BNC/Micelle conjugate and $\alpha v\beta_3$ integrin receptor

3.1 BNC Encapsulation in PEG-Modified Phospholipid Micelles

The '*as prepared*' organic capped BNCs, investigated by TEM analysis, have shown that each BNC is formed by a rod attached to a sphere, according to the morphology previously reported (Fig. 2a) [19, 28].

In the inset of Fig. 2a, the size distribution of the two phases in BNCs clearly highlights a mean particle size of 8 nm (σ%=15%) for the iron oxide particles and a mean particle length for TiO_2 NRs of 18 nm (σ%=10%). The optical characterization of the organic capped BNCs has been performed by UV-Vis absorption spectroscopy.

In Fig. 2b, the absorption spectrum of pure TiO_2 NRs has been compared to that of BNCs. Bare TiO_2 NRs absorb mainly in the UV spectral region, below 400 nm, due to the intrinsic band gap of anatase-TiO_2 (3.2 eV). Conversely, the absorption edge threshold of BNCs is clearly shifted towards the visible region due to the narrow band gap of maghemite (2.3 eV) [24, 26].

Therefore, the combination of the magnetic domain with theTiO_2 NRs in the BNC structure enables an extension of light absorption in the visible range of the spectrum, thus providing a significant advantage over the use of bare TiO_2 nanostructures as photosensitizer for the PDT therapy.

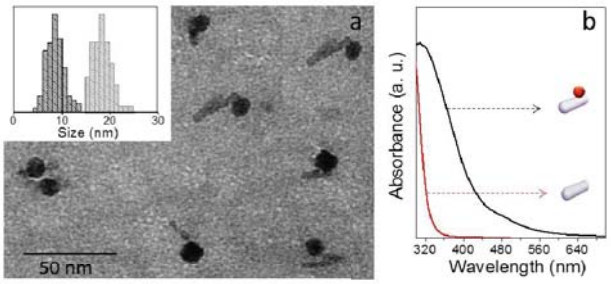

Figure 2 TEM micrograph of organic capped BNCs cast from chloroform (a) Particle size distribution of (gray) TiO_2 NRs and (black) Fe_2O_3 NCs (inset a) NCs. Absorption spectra of organic capped pure TiO_2 NRs (red line) and BNCs (black line) in chloroform solution. Concentration of pure TiO_2 NRs and BNCs in chloroform of $5*10^{-4}$ M (b)

The organic capped BNCs have been then encapsulated within PEG-modified phospholipids micelles, and thus, exploiting hydrophobic interactions between the pristine capping ligand of BNCs and the hydrophobic tails of lipids, dispersibility of the heterostructure in aqueous media has been achieved. In addition, as previously demonstrated, the BNC encapsulation process in phospholipid micelles does not affect the magnetic properties of the *as-synthesized* BNCs, which resulted in superparamagnetic regime at room temperature [19].

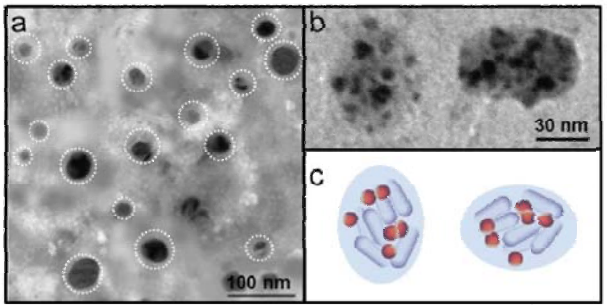

Figure 3 TEM micrographs with positive (a) and negative (b) staining for BNC/Micelles dispersed in aqueous PBS buffer. Schematic sketch (c) of BNCs encapsulated in the hydrophobic core of PEG-modified phospholipid micelles

A structural investigation of the BNC encapsulating micelles has been performed by TEM and DLS analysis. TEM micrograph with positive staining of the BNC/Micelles, reported in Fig. 3a, clearly indicates that the micelle

diameter ranges from 15 to 70 nm, pointing outthe formation of aggregates in a wide range of sizes, containing a variable number of BNCs clustered in a single micelle. This result has been confirmed by DLS analysis that clearly points out a bimodal size distribution (Fig. 4a, blue line). Small aggregates with an average hydrodynamic diameter of 18 nm coexist with larger aggregates with an average hydrodynamic diameter of 77 nm (PDI=0.283±0.007). The size of the small aggregates is indeed compatible with that found for the empty micelles (Fig. S1, Supporting Information), that concomitantly form during the BNC micelle process. Conversely, the presence of population with a larger average hydrodynamic diameter can be explained assuming that clusters of a variable number of BNCs can be embedded within one single micelle [19].

ζ-potential measurements on the BNC/Micelle samples have resulted in an average ζ-potential value of (-18.3±0.6) mV, thus indicating a good colloidal stability of the investigated system (Fig. 4b, blue line).

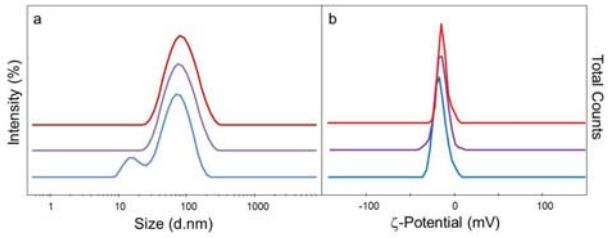

Figure 4 Size distribution by intensity (a) and ζ-potential analysis for BNC/Micelles (blue line) $(GK)_2$-DNS peptide/ BNC/Micelle conjugates (purple line) and RGD$(GK)_2$-DNS peptide/ BNC/Micelles conjugates (red line)

3.2 Bioconjugation of BNC/Micelles with $(GK)_2$-DNS

The formation of amide bonds between the exposed carboxylic groups of BNC/PEG lipid micelles and the primary amine groups of peptide, has been promoted by means of the sulfo-NHS and EDC reaction to achieve the bioconjugation. A systematic study by using the $(GK)_2$-DNS peptide, which contains two amino groups and one DNS moiety for molecule, has been initially carried out in order to identify the appropriate chemical conditions, such as reagent concentration and reaction time, for a successful coupling (Fig. 1a).

As an alternative to the more conventional EDC/sulfo-NHS two steps coupling reaction, a one-step conjugation reaction of BNC/Micelles with $(GK)_2$-DNS peptide has been preliminarily performed by adding all of the reagent in one pot, in PBS buffer at pH 7.2. Indeed, such one step conjugation procedure, which can be successfully employed for small proteins, peptides or DNA oligomers, represents a fast and effective method to achieve desired degree of optimization for the coupling reaction. The effective coupling, has been quantitatively evaluated as a function of the reaction parameters, by means a calibration curve and measuring emission of the sample, due to the presence of the fluorescent DNS group in the peptide structure, which exhibits an emission band centered at 560 nm in aqueous PBS buffer (Inset Fig. 5a, red line).

The reaction conditions have been first explored by tuning $(GK)_2$-DNS peptide concentration in the range between $1.0*10^{-4}$ and $1.0*10^{-3}$ M, keeping constant the molar ratio of EDC/sulfo-NHS at 1:2.5. The concentration of carboxylic groups on BNC/Micelle surface has been fixed at value of $5*10^{-4}$ M and finally, the reaction mixture has been stirred for 2 h at room temperature (Table 1). The amount of $(GK)_2$-DNS peptide covalently linked to BNC/micelle surface has been estimated to be of 112±4, 178±4, 174±4 and 177±4 μg/mL for the bioconjugated sample prepared starting from a peptide concentration of $1.0*10^{-4}$, $1.5*10^{-4}$, $5*10^{-4}$ and $1*10^{-3}$ M, respectively. The obtained data show that the coupling yield grows by increasing the peptide concentration from $1.0*10^{-4}$ to $1.5*10^{-4}$ M, but also that the conjugation yield does not increase further by rising the peptide concentration above the value of $1.5*10^{-4}$M, under the same experimental conditions. In addition, when a higher concentration ($1*10^{-3}$ M) of carboxylic groups has been investigated, by

keeping constant the molar ratio of EDC/Sulfo-NHS (1:2.5) and fixing the $(GK)_2$-DNS peptide at value of $1.5*10^{-4}$ M, a concentration of the peptide bound to BNC/micelle surface of 176±4 μg/mL has been attained, thus resulting, also in this case, in no significant improvement of the coupling yield. Finally, the incubation time has been also investigated to assess whether and how may affect the degree of coupling. The incubation time has been increased in the bioconjugation reaction from 2, to 7 and up to 18 hours, keeping constant the concentration of carboxylic groups, EDC, Sulfo-NHS and $(GK)_2$-DNS peptide at $5*10^{-4}$, $5*10^{-3}$, $1.25*10^{-2}$ and $1.5*10^{-4}$ M, respectively. The PL measurements have resulted in a $(GK)_2$-DNS peptide concentration of 175 ± 4, 176 ± 4 and 173 ± 4 μg/mL for bioconjugates obtained at incubation time of 3, 7 and 18 h, respectively.

Table 1 Summary of the investigated experimental conditions for the coupling reaction by varying the $(GK)_2$-DNS peptide concentration

[-COOH] (M)	[EDC] (M)	[Sulfo-NHS] (M)	[(GK)2-DNS Peptide] (M)	$t_{reaction}$ (hr)
5.10^{-4}	5.10^{-3}	$1.25.10^{-2}$	$1.0.10^{-4}$	2
5.10^{-4}	5.10^{-3}	$1.25.10^{-2}$	$1.5.10^{-4}$	2
5.10^{-4}	5.10^{-3}	$1.25.10^{-2}$	$5.0.10^{-4}$	2
5.10^{-4}	5.10^{-3}	$1.25.10^{-2}$	1.10^{-3}	2

These results point out that the coupling reaction takes place already in the first 2 hours and that the most advantageous coupling conditions can be realized by using a concentration of carboxylic groups, EDC, sulfo-NHS and (GK)2-DNS peptide of $5*10^{-4}$, $5*10^{-3}$, $1.25*10^{-2}$ and $1.5*10^{-4}$ M, respectively. Any further increase of peptide or carboxylic group concentration does not improve the efficiency of the coupling reaction, probably due to a steric hindrance effect on BNC/Micelle surface.

Since bioconjugation reaction has been performed in excess of peptide, a purification procedure has been required, and its efficiency has been investigated by means of HPLC analysis, using UV-Vis and fluorescence detectors (Fig. 5b).

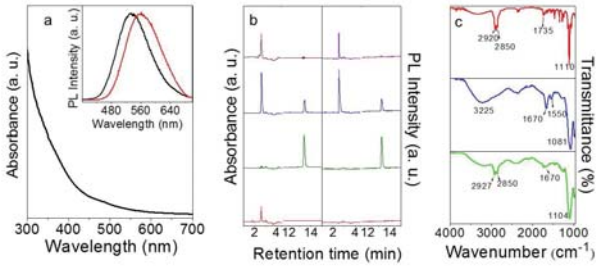

Figure 5 UV-Vis absorption spectrum of $(GK)_2$-DNS peptide/BNC/Micelle conjugates (a). PL emission spectra of free $(GK)_2$-DNS peptide (red line) and of $(GK)_2$-DNS peptide/BNC/Micelle conjugates (black line, λ_{ex} 329 nm) (Inset in panel a). HPLC chromatograms obtained from BNC/Micelles (red line), pure $(GK)_2$-DNS peptide (green line), non purified $(GK)_2$-DNS peptide/BNC/Micelle conjugates (blue line) and purified $(GK)_2$-DNS peptide/BNC/Micelle bioconjugates (purple line) by UV absorption at 230 nm (b, left panel) and fluorescence at 560 nm, λ_{ex} 329 nm (b, right panel). FTIR-ATR spectra of BNC/Micelles (red line), free $(GK)_2$-DNS peptide (blue line) and $(GK)_2$-DNS peptide/BNC/Micelles conjugates (green line), all cast from PBS aqueous solution (c)

PBS buffer, free $(GK)_2$-DNS peptide, BNC/Micelles, non purified and purified $(GK)_2$-DNS peptide/BNC/Micelle conjugates have been injected by using an aqueous mobile phase containing 5% of ACN and by using a C18 column (Phenomenex Synergi 4μm Hydro-RP 80A C-18). After 2 min, the percentage of ACN has been raised from 5 to 100% over 15 min. The chromatogram with UV-Vis detection obtained from the BNC/Micelles reports only a peak eluted at 2.6 min, and no PL signal has been detected upon elution by using fluorescence detector (Fig. 5b, red line). The elution profile of the pure peptide (Fig. 5b, green line) exhibits only an absorption peak at 13.3 min, which is also present in the chromatogram obtained by using fluorescence detector. The PL signals have been recorded at 560 nm (λ_{ex} 329 nm), which is the wavelength of emission maximum in the PL spectrum of the pure $(GK)_2$-DNS peptide (Inset Fig. 5a, red line). In the chromatogram obtained from non purified $(GK)_2$-DNS peptide/BNC/Micelle conjugates, two peaks, at elution time of 2.6 and 13.3 min can be observed. The peak at earlier elution time can be reasonably ascribed to BNC/Micelles conjugated with $(GK)_2$-DNS peptide.

This assignment is justified by the elution profile recorded performing the PL detection at 560 nm, which reveals a peak at 2.3 m, assigned to the peptide covalently linked to BNC/Micelle surface. Conversely, the peak at 13.3 m, clearly detected in both chromatograms, using either UV-Vis and PL detection, can be reasonably ascribed to the excess of pure peptide (Fig. 5b, blue line). In the chromatogram of purified $(GK)_2$-DNS peptide/BNC/Micelle conjugates, only the UV and PL signals of peptide conjugated to BNC/Micelle can be detected, while the signals attributable to the pure peptide disappear, thus suggesting that the excess of peptide has been effectively removed (Fig. 5b, purple line).

The $(GK)_2$-DNS peptide/BNC/Micelles conjugates have been comprehensively characterized by means of complementary optical (UV-Vis, PL, FT-IR and DLS) techniques. The absorbance spectrum of the BNC conjugates recalls that of the *'as synthesized'* BNCs. The characteristic peaks of the $(GK)_2$-DNS peptide at 213, 246 and 328 nm (Fig. S2, Electronic Supplementary Information) cannot be detected, as they are expected in the region that is, in fact, dominated by the absorption band of the BNCs (Fig. 5a). Conversely, in the PL spectrum of bioconjugates (Inset Fig. 5a, black line) the presence of the emission band centered at 532 nm can be clearly observed, being certainly ascribable to the peptide that is covalently linked to the BNC/Micelle surface and that contains the DNS group as fluorescent probe. The shift of emission maximum wavelength from 560 nm for the pure $(GK)_2$-DNS peptide (Inset Fig. 5a, red line) to 532 nm for the bioconjugate can be reasonably assigned to the micellar environment around the probe, which is particularly sensitive to any change of the polarity of the surrounding medium [29, 30].

Further investigation has been carried out by FT-IR spectroscopy, and the results are shown in Fig. 5c for BNC/Micelles (red line), free $(GK)_2$-DNS peptide (blue line) and $(GK)_2$-DNS peptide/ BNC/Micelles conjugates (green line). In the FTIR-ATR spectrum of BNC/Micelles, the C–H stretching modes are evident in the 3000–2805 cm^{-1} region; the peak at 1735 cm^{-1} can be attributed to the C=O stretching and the band centered at 1100 cm^{-1} is due to the C–O–C ether stretching, univocally ascribable to the PEG lipids. In the FTIR-ATR spectrum of the free $(GK)_2$-DNS peptide, the band located at 3225 cm^{-1} is due to the N–H stretching, while the Amide I and II bands have been found to have maximum peaks at 1670 and 1550 cm^{-1}. In the 1200 and 1000 cm^{-1} region, the band centered at 1081 cm^{-1} can be assigned to symmetrical stretching vibrations of SO_2 and of $N\text{-}(CH_3)_2$, such as also to in-plane aromatic C-H bending vibration of DNS moiety [31]. The FTIR-ATR spectrum of the $(GK)_2$-DNS peptide/BNC/Micelles conjugates corresponds to the sum of the free $(GK)_2$-DNS and BNC/Micelle spectra, where the Amide I mode is still present, thus confirming the occurrence of the bioconjugation reaction. In addition, the band, that is located at 1081 cm^{-1} in the free peptide spectrum, appears shifted of about 23 cm^{-1} in the $(GK)_2$-DNS peptide/BNC/Micelle conjugate spectrum, owing to the additional presence of the C–O–C ether stretching in the 1200 and 1000 cm^{-1} region.

DLS investigation on $(GK)_2$-DNS peptide/BNC/Micelle conjugate samples has revealed a monomodal size distribution and an average hydrodynamic diameter of 80 nm (PDI = 0.188 ± 0.002), suggesting that the empty micelles, whose formation occurs during the BNC/Micelle preparation (Fig. 4 a, blue line), have been completely removed after purification procedure of the bioconjugates (Fig. 4a, purple line). Furthermore, the good colloidal stability of the $(GK)_2$-DNS peptide/BNC/Micelle conjugates has been highlighted by means ζ-potential measurements that have resulted in an average ζ-potential value of -17.1 ± 0.9 mV (Fig. 4b, purple line).

Finally, in order to rule out any non specific absorption of the peptide on PEG-lipid micelle surface, a mixture containing BNC/micelles and free $(GK)_2$-DNS peptide, without any linker, has been incubated for two hours, under the same optimized experimental conditions for the preparation of the $(GK)_2$-DNS peptide/BNC conjugates (-COOH and peptide concentration of $5*10^{-4}$ and $1.5*10^{-4}$ M, respectively). After the purification, PL measurements performed on the recovered precipitate have pointed out that no emission band can be clearly assigned to DNS group, which is, conversely, clearly evident in the

PL spectrum of $(GK)_2$-DNS peptide/BNC conjugates (Fig. S3, Electronic Supplementary Information), thus indicating the formation of a covalent bond when the bioconjugation reaction has been carried out in presence of cross linking agents, as previously described.

3.3 Bioconjugation of BNC/Micelles with RGD$(GK)_2$-DNS Peptide

The covalent binding of RGD$(GK)_2$-DNS peptide at the BNC/Micelle surface has been performed under the optimized experimental conditions (concentration of –COOH groups, EDC, sulfo-NHS and $(GK)_2$-DNS peptide of $5*10^{-4}$, $5*10^{-3}$, $1.25*10^{-2}$ and $1.5*10^{-4}$ M, respectively) defined for the conjugation of $(GK)_2$-DNS peptide. In the case of the RGD$(GK)_2$-DNS peptide, the coupling reaction has been performed in two steps, in order to improve the efficiency of the conjugation and to avoid the activation of carboxylic group in the RGD cyclic sequence of the peptide by removing, after the first step, the excess of the two crosslinking agents. The concentration of RGD$(GK)_2$-DNS peptide conjugated to BNC/micelle surface has been estimated, by PL measurements, to be 98 ± 4 μg/mL, which is a value lower than that obtained for the $(GK)_2$-DNS peptide, reasonably due to a higher steric hindrance of the RGD$(GK)_2$-DNS peptide molecules available for binding at BNC/micelle surface, thus reducing the coupling reaction yield.

The RGD$(GK)_2$-DNS peptide/BNC/Micelle bioconjugates have been characterized by DLS investigation, ζ-potential measurements (Fig. 4, red line) and FTIR-ATR analysis (Fig. S4, Electronic Supplementary Information). In Fig. 4a (red line), a monomodal size distribution with an average hydrodynamic diameter of 81 nm (PDI = 0.108 ± 0.003) can be clearly observed; ζ-potential value of -16.6 ± 0.26 mV has been recorded, since the arginine residue in the RGD$(GK)_2$-DNS peptide probably slightly reduces the negative charge on the bioconjugate surface (Fig. 4b, red line).

3.4 In vitro cytotoxicity and cellular uptake studies

The effect of the BNC containing micelles, before and after their covalent binding to RGD$(GK)_2$-DNS peptide, on the viability of MCF-7 and WM266 cells has been assessed by performing an *in vitro* toxicity evaluation after a long-term exposure of cells to increasing concentration of BNC/Micelles and RGD$(GK)_2$-DNS peptide/BNC/Micelle conjugates. Cell viability has been assessed by the MTT assay. For this purpose, the average concentration values of γ-Fe_2O_3 and TiO_2, in the both BNC/Micelle and bioconjugate samples, have been previously estimated by colorimetric analysis and anodic stripping voltammetry, respectively (Table 2).

Table 2 Concentration of γ-Fe_2O_3 by colorimetric analysis and of TiO_2 by anodic stripping voltammetry in BNC/Micelles and BNC/Micelles conjugated with RGD-$(GK)_2$-DNS-peptide. Data presented as mean ± standard error (three replicates)

	[γ-Fe_2O_3] (μg/mL)	[TiO_2] (μg/mL)
BNC/Micelles	184 ± 5	50 ± 5
RGD(GK)2-DNS Peptide/BNC/Micelles Conjugates	170 ± 15	44 ± 5

The obtained data reveal no significant difference both in γ-Fe_2O_3 and TiO_2 content passing from BNC/Micelles to conjugate samples, as reasonably expected.

WM266 cells, human malignant melanoma cells expressing high levels of $\alpha v\beta_3$ integrin [32] have been selected as targeted cells to carry out the cytotoxicity studies. In addition, MCF-7 breast cancer cells, which express the integrin $\alpha v\beta 3$ at very low level [17, 33] have been tested as control group. In particular, WM266 and MCF-7 cells have been incubated with BNC/Micelles and peptide/BNC/Micelle conjugates at γ-Fe_2O_3 concentration values ranging from $2.27*10^{-6}$ to 0.113 mg/mL (TiO_2 concentration range from $2.93*10^{-2}$ to $5.87*10^{-7}$ mg/mL) for 72 hours.

As clearly shown in Fig. 6a and b, no significant effect on cell viability can be observed when the WM266 and MCF-7 cells have been incubated with BNC/Micelles and RGD$(GK)_2$-DNS peptide/BNC/Micelle conjugates at γ-Fe_2O_3 concentration values ranging from $2.27*10^{-6}$ to $2.27*10^{-4}$ mg/mL. Above the γ-Fe_2O_3 concentration value of $2.27*10^{-4}$ mg/mL, the BNC/Micelles and RGD$(GK)_2$-DNS peptide/BNC/Micelle conjugates have affected the cell viability in a

concentration-dependent way for the both WM266 and MCF-7 cells, giving the IC_{50} values reported in Fig. 6 c. In the case of MCF-7 cells, the IC_{50} values are (0.0095±0.0020) mg/mL for the BNC/Micelles and (0.0055±0.0032) mg/mL for RGD-peptide/BNC/Micelle conjugates, respectively, thus indicating that no statistically significant difference in citotoxicity can be observed for the BNC/Micelles before and after their conjugation with RGD(GK)$_2$-DNS peptide.

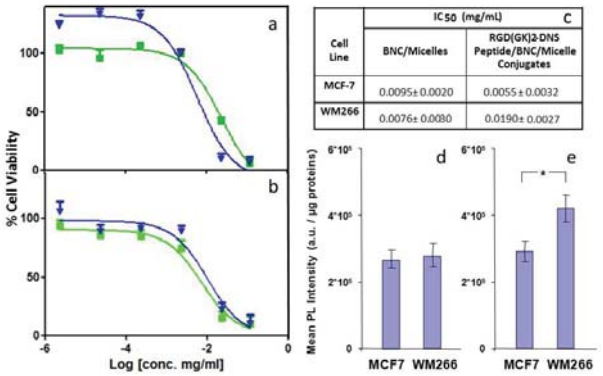

Cell Line	IC50 (mg/mL) c	
	BNC/Micelles	RGD(GK)2-DNS Peptide/BNC/Micelle Conjugates
MCF-7	0.0095± 0.0020	0.0055 ± 0.0032
WM266	0.0076± 0.0080	0.0190± 0.0027

Figure 6 Viability results for WM266 (a) and MCF-7 (b) cells after incubation for 72 h with BNC/Micelles (blue line) or RGD(GK)$_2$-DNS peptide/BNC/Micelle conjugates (green line), respectively. IC_{50} values, resulting from the same viability assays, expressed as γ-Fe_2O_3 concentration. Data presented as mean ± standard error of three distinct experiments performed in triplicate (c). Mean PL intensity (expressed as a. u./ µg protein) of cell lysates recovered from MCF-7 and WM266 cells incubated with (GK)$_2$-DNS Peptide/BNC/Micelle conjugates (d) and RGD(GK)$_2$-DNS peptide/BNC/Micelle conjugates (e) at γ-Fe_2O_3 concentration of $2.27*10^{-3}$ mg/mL for 12 h. Values expressed as the mean ± standard error of three separate experiments performed in triplicate. Statistical significance analyzed using Student's t-test (*$p < 0.05$) (d)

Conversely, in WM266 cells, expressing $\alpha v\beta_3$ integrin, the cytotoxic activity of RGD(GK)$_2$-DNS peptide/BNC/Micelle conjugates has been found slightly lower than that of BNC/Micelles, as highlighted by the corresponding IC_{50} values, expressed as γ-Fe_2O_3 concentration, namely (0.0076 ±0.0030) mg/mL for the BNC/Micelles and (0.0190 ± 0.0027) mg/mL for the RGD-peptide/BNC conjugates, respectively (Fig. 6 c). The different cytotoxic behavior observed for the two cell lines could be reasonably due to diverse pathways and mechanism involved in the endocytic process of the RGD(GK)$_2$-DNS peptide/BNC/Micelle conjugates. The evaluation of the cellular uptake of (GK)$_2$-DNS peptide/BNC/Micelle and RGD(GK)$_2$-DNS peptide/BNC/Micelle conjugates in the WM266 and MCF-7 cells has been carried out by comparing PL emission intensity data in cell lysates. In particular, WM266 and MCF-7 cells have been incubated with (GK)$_2$-DNS peptide/BNC/Micelle and RGD(GK)$_2$-DNS peptide/BNC/Micelle conjugates, for 12 hours at γ-Fe_2O_3 concentration value of $2.27*10^{-4}$ mg/mL, which resulted to be not cytotoxic for the both cell lines and the peptide-conjugates, with and without RGD motif (Fig. 6a, green line, Table S1 Electronic Supplementary Information).

Fig. 6 e clearly shows that, when the cells have been incubated with RGD(GK)$_2$-DNS peptide/BNC/Micelle conjugates, the mean PL intensity in cell lysates of WM266 cells (expressed as a. u./ µg protein and calculated as described in experimental section) results significantly higher (44%) than that of recorded for cell lysates of MCF-7 cells. On contrary, no significant difference in the mean PL intensity in cell lysates of the two different cell lines, both incubated with (GK)$_2$-DNS peptide/BNC/Micelle conjugates, can be observed (Fig. 6 d). Since PL signal recorded in lysates can be unambiguously attributed to the DNS group of the peptide covalently bound to BNC/Micelle surface, these results point out the cell entry ability of the two peptide-conjugates, with and without the RGD sequence, in the both MCF-7 and WM266 cells, although a more efficient uptake of the RGD(GK)$_2$-DNS peptide/BNC/Micelle conjugates has been observed for the WM266 cell line, in agreement with its very high surface expression of the appropriate receptor for RGD-motif.

Indeed RGD-based peptides nanosystems have been already well documented as able to cross the cell membrane both by passive diffusion and receptor mediated endocytosis [32, 34, 35]. Consequently, it is reasonable to assign the PL signal recorded for the WM266 cells to a receptor mediated endocytosis of (RGD(GK)$_2$-DNS peptide/BNC/Micelle conjugates, although a passive (EPR-mediated) transport seems to occur concomitantly.

Such an explanation is further supported by the values obtained for the PL signal detector for the lysates recovered from MCF-7 cell line incubated with the (GK)$_2$-DNS peptide/BNC/Micelle and

RGD(GK)$_2$-DNS peptide/BNC/Micelle conjugates and from the WM266 cells after incubation with the (GK)$_2$-DNS peptide/BNC/Micelle. The comparable PL signals recorded in these latter cases suggest the occurrence of the cellular uptake mainly by a passive diffusion. Conversely, the higher mean PL intensity obtained for the WM266 cells, where high levels of the $\alpha v\beta_3$ receptor are overexpressed, indicates a significant selectivity of the RGD(GK)$_2$-DNS peptide/BNC/Micelle conjugates for the $\alpha v\beta_3$ integrin [32, 34].

Further evidence of the effective uptake of RGD(GK)$_2$-DNS peptide/BNC/Micelle conjugates in WM266 cells has been also demonstrated by confocal microscopy investigation (Fig. 7).

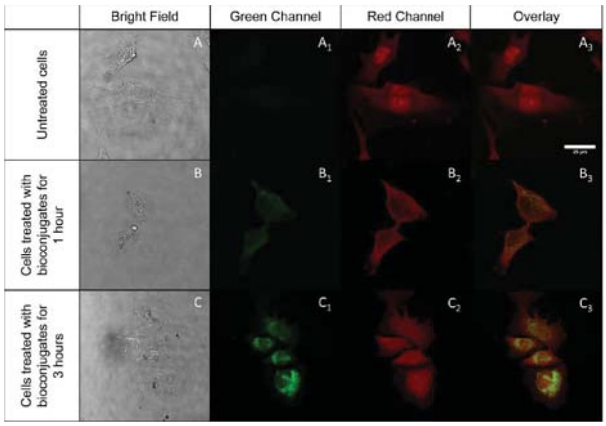

Figure 7 Confocal bright field and fluorescence micrographs of fixed WM266 cells. Time-dependent uptake of RGD(GK)$_2$-DNS peptide/BNC/Micelle conjugates by WM266 cells. Control: untreated cells (Panel A, A1, A2, A3). Cells images after 1 (Panel B, B1, B2, B3) and 3 hours (Panel C, C1, C2, C3) respectively, of incubation time with RGD(GK)$_2$-DNS peptide/BNC/Micelle conjugates. Cells images in the bright field (Panel A, B, C), green (Panel A1, B1, C1) and red detection channel (Panel A2, B2, C2). Overlay of green and red fluorescence (Panel A3, B3, C3). Scale bar 25 μm.

The cells have been incubated with conjugate samples at concentration of $2.27*10^{-3}$ mg/mL for 1 (Fig. 7, Panel B, B1, B2, B3), 3 (Fig. 7, Panel C, C1, C2, C3) and 24 hours, respectively (data not shown), fixed and treated with Phalloidin-TRIC, able to stain the F-actin cytoskeleton of the cells. The individual green and red PL of RGD(GK)$_2$-DNS peptide/BNC/Micelle conjugates and Phalloidin-TRIC, in fixed WM266 cells, are demonstrated in the panels B1, C1 and panels B2, C2 of Fig. 7, respectively. Panels A1 and A2 (Figure 7) reveal that only red PL of Phalloidin-TRIC can be observed in untreated cells, while no green autofluorescence signal can be detected. Association between the green and red is evident in the overlays of panels A3, B3 and C3. The observations made in cellular imaging experiments clearly prove that the RGD(GK)$_2$-DNS peptide/BNC/Micelle conjugates are able to enter the cells (Panel B3 and C3, Fig. 7) and that their uptake is dependent on the time incubation. Indeed, increased green PL in the cells has been detected by increasing the incubation time with bioconjugates (Panel B1 and C1, Fig. 7). Interestingly, the images of the WM266 cells treated with bioconjugate samples for 3 hours clearly indicate the accumulation of green emitting endocytic vesicles in subcellular compartments (Fig. 7 C-C3 and Fig. 8).

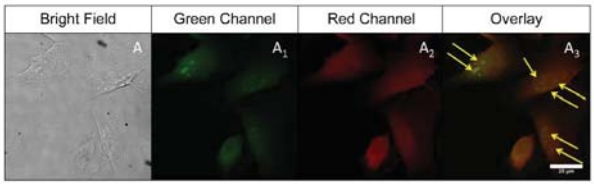

Figure 8 Confocal bright field and fluorescence micrographs of a close up of Figure 7 C. WM266 cells images in the bright field (Panel A), green (Panel A1) and red (Panel A2) detection channel, after 3 h of incubation time with RGD(GK)$_2$-DNS peptide/BNC/Micelle conjugates. Overlay of green and red fluorescence (Panel A3). Scale bar 25 μm

4. CONCLUSIONS

Multifunctional heterostructures consisting of a semiconductor TiO_2 NR joined to a magnetic γ-Fe_2O_3 spherical domain, synthesized with high control on their size and shape, have been embedded in the hydrophobic core of PEG-terminated phospholipid micelles, obtaining BNCs with elevated dispersibility and stability in aqueous solution.

Subsequently, the BNC/Micelles have been conjugated with two different fluorescent peptides, namely RGD(GK)$_2$-DNS and (GK)$_2$-DNS peptide. The (GK)$_2$-DNS peptide has been used to preliminary scan and set up the experimental conditions, such as reagent concentrations and reaction time for the bioconjugation process, and used as control systems to evaluate the effect of the

RGD sequence on the selective targeting of the $\alpha v\beta_3$ integrin.

Complementary optical and structural techniques have provided a comprehensive characterization of the bioconjugate samples, demonstrating the effective bioconjugation, and their high stability in aqueous medium.

Cytotoxic activity of the BNC/Micelles and RGD$(GK)_2$-DNS peptide/ BNC/Micelle conjugates on MCF-7 and WM266 cell lines, respectively, has been shown only for the highest value of the tested concentrations (above $2.27*10^{-4}$ mg/mL), and after a long-term exposure of cells. PL intensity measures after cell lysis along with confocal microscopy have highlighted the ability of RGD$(GK)_2$-DNS peptide/BNC/Micelle conjugates to be internalized. The experimental evidence indicates that the uptake of peptide conjugated with RGD motif by WM266 cells, reasonably occur not merely by passive (EPR-mediated) transport, but significantly involves also a receptor-mediated endocytosis. This evidence points out the selectivity of the employed RGD-peptide for targeting $\alpha v\beta_3$ integrin. However, further deeper investigations are needed to establish the exact mechanism by which the RGD functionalized bioconjugates enter the cells.

The proposed approach allows to achieve stable functional peptide/BNC conjugates that have a large potential in theranostic application, including targeted imaging and treatment of cancer. Indeed the magnetic and RGD domains can be both effective in directing the conjugates toward tumor tissues, where MRI and magnetically induced hyperthermia will be able to effectively operate, in combination with TiO_2-based photodynamic therapy, in a single multifunctional nanoplatform.

Finally the proposed bioconjugation paradigm with such targeting peptides, can be reasonably extended to other functional inorganic nanocrystals, and to diverse peptide motifs, thus further widening the potential and versatility of nanomaterials for biomedical applications.

Acknowledgements

The authors grateful acknowledge Mr. Domenico Benedetti for Anodic Stripping Voltammetry measurements and colorimetric analysis.

The work has been supported by PRIN 2010-2011 (2010C4R8M8), PON R&C 2007–2013 MAAT-Molecular Nanotechnology for Health and Environment (Project number: PON02_00563_3316357), FIRB Futuro in Ricerca (RBFR122HFZ), FIRB project "Integrated Network for Nano-Medicine (RINAME)" RBAP114AMK_006, Nanomax-integrable sensors for pathological biomarkers diagnosis (N-CHEM), Laboratorio Regionale di Sintesi e Caratterizzazione di Nuovi Materiali Organici e Nanostrutturati per Elettronica, Fotonica e Tecnologie Avanzate, National and Sens&Micro LAB (POFESR 2007–2013) projects.

Electronic Supplementary Material: Optical characterization by UV-Vis absorption and PL spectroscopy of free (GK)2-DNS peptide, DLS investigation performed on empty micelles, FTIR-ATR analysis of free RGD(GK)2-DNS peptide and RGD(GK)2-DNS peptide/BNC conjugates, and viability results for WM266 and MCF-7 cells after incubation with (GK)2-DNS peptide/BNC/Micelle conjugates have been also performed and reported. Furthermore, a control test has been performed to rule out any non specific absorption of the peptide on PEG-lipid micelle surface during the bioconjugation process. Supplementary material is available in the online version of this article at http://dx.doi.org/10.1007/s12274-***-****-*

References

[1] Park, K.; Lee, S.; Kang, E.; Kim, K.; Choi, K.; Kwon, I. C. New generation of multifunctional nanoparticles for cancer imaging and therapy. *Advanced Functional Materials* **2009**, *19*, 1553-1566.

[2] Bardhan, R.; Lal, S.; Joshi, A.; Halas, N. J. Theranostic nanoshells: from probe design to imaging and treatment of cancer. *Accounts of chemical research* **2011**, *44*, 936-946.

[3] Fu, A.; Wilson, R. J.; Smith, B. R.; Mullenix, J.; Earhart, C.; Akin, D.; Guccione, S.; Wang, S. X.; Gambhir, S. S. Fluorescent magnetic nanoparticles for magnetically enhanced cancer imaging and targeting in living subjects. *ACS Nano* **2012**, *6*, 6862-6869.

[4] Bertrand, N.; Wu, J.; Xu, X.; Kamaly, N.; Farokhzad, O. C. Cancer nanotechnology: the impact of passive and active targeting in the era of modern cancer biology. *Adv. Drug Deliv. Rev.* **2014**, *66*, 2-25.

[5] Banerjee, D.; Harfouche, R.; Sengupta, S. Nanotechnology-mediated targeting of tumor

angiogenesis. *Vascular cell* **2011**, *3*, 3-13.

[6] Montet, X.; Montet-Abou, K.; Reynolds, F.; Weissleder, R.; Josephson, L. Nanoparticle imaging of integrins on tumor cells. *Neoplasia* **2006**, *8*, 214-222.

[7] Ye, Y.; Chen, X. Integrin targeting for tumor optical imaging. *Theranostics* **2011**, *1*, 102-126.

[8] Danhier, F.; Le Breton, A.; Preat, V. RGD-based strategies to target alpha(v) beta(3) integrin in cancer therapy and diagnosis. *Mol. Pharm.* **2012**, *9*, 2961-2973.

[9] Scari, G.; Porta, F.; Fascio, U.; Avvakumova, S.; Dal Santo, V.; De Simone, M.; Saviano, M.; Leone, M.; Del Gatto, A.; Pedone, C.; Zaccaro, L. Gold nanoparticles capped by a GC-containing peptide functionalized with an RGD motif for integrin targeting. *Bioconjugate chemistry* **2012**, *23*, 340-349.

[10] Lee, J.; Lee, T. S.; Ryu, J.; Hong, S.; Kang, M.; Im, K.; Kang, J. H.; Lim, S. M.; Park, S.; Song, R. RGD peptide-conjugated multimodal NaGdF4:Yb3+/Er3+ nanophosphors for upconversion luminescence, MR, and PET imaging of tumor angiogenesis. *Journal of nuclear medicine: official publication, Society of Nuclear Medicine* **2013**, *54*, 96-103.

[11] Zhang, F.; Huang, X.; Zhu, L.; Guo, N.; Niu, G.; Swierczewska, M.; Lee, S.; Xu, H.; Wang, A.Y.; Mohamedali, K. A.; Rosenblum, M. G.; Lu, G.; Chen, X. Noninvasive monitoring of orthotopic glioblastoma therapy response using RGD-conjugated iron oxide nanoparticles. *Biomaterials* **2012**, *33*, 5414-5422.

[12] Shi, P.; Chen, H.; Cho, M.R.; Stroscio, M. A. Peptide-directed binding of quantum dots to integrins in human fibroblast. *IEEE transactions on nanobioscience* **2006**, *5*, 15-9.

[13] Chen, H.; Wang, L.; Yeh, J.; Wu, X.; Cao, Z.; Wang, Y. A.; Zhang, M.; Yang, L.; Mao, H. Reducing non-specific binding and uptake of nanoparticles and improving cell targeting with an antifouling PEO-b-PgammaMPS copolymer coating. *Biomaterials* **2010**, *31*, 5397-5407.

[14] Wang, C.; Bao, C.; Liang, S.; Fu, H.; Wang, K.; Deng, M.; Liao, Q.; Cui, D. RGD-conjugated silica-coated gold nanorods on the surface of carbon nanotubes for targeted photoacoustic imaging of gastric cancer. *Nanoscale research letters* **2014**, *9*, 264.

[15] Nazli, C.; Ergenc, T. I.; Yar, Y.; Acar, H. Y.; Kizilel, S. RGDS-functionalized polyethylene glycol hydrogel-coated magnetic iron oxide nanoparticles enhance specific intracellular uptake by HeLa cells. *International journal of nanomedicine* **2012**, *7*, 1903-1920.

[16] Gao, J.; Chen, K.; Xie, R.; Xie, J.; Yan, Y.; Cheng, Z.; Peng, X.; Chen, X. In vivo tumor-targeted fluorescence imaging using near-infrared non-cadmium quantum dots. *Bioconjugate chemistry* **2010**, *21*, 604-609.

[17] Yin, H. Q.; Mai, D.; Gan, F.; Chen, X. One-step synthesis of linear and cyclic RGD conjugated gold nanoparticles for tumour targeting and imaging. *RSC Advances* **2014**, *4*, 9078-9085.

[18] Arosio, D.; Manzoni, L.; Araldi, E. M.; Scolastico, C. Cyclic RGD functionalized gold nanoparticles for tumor targeting. *Bioconjugate chemistry* **2011**, *22*, 664-672.

[19] Depalo, N.; Carrieri, P.; Comparelli, R.; Striccoli, M.; Agostiano, A.; Bertinetti, L.; Innocenti, C.; Sangregorio, C.; Curri, M. L. Biofunctionalization of anisotropic nanocrystalline semiconductor-magnetic heterostructures. *Langmuir: the ACS journal of surfaces and colloids* **2011**, *27*, 6962-6970.

[20] Santhosh, P. B.; Ulrih, N. P. Multifunctional superparamagnetic iron oxide nanoparticles: promising tools in cancer theranostics. *Cancer letters* **2013**, *336*, 8-17.

[21] Hao, R.; Xing, R.; Xu, Z.; Hou, Y.; Gao, S.; Sun, S. Synthesis, functionalization, and biomedical applications of multifunctional magnetic nanoparticles. *Advanced materials* **2010**, *22*, 2729-2742.

[22] Yin, Z. F.; Wu, L.; Yang, H.G.; Su, Y. H. Recent progress in biomedical applications of titanium dioxide. *Physical chemistry chemical physics: PCCP* **2013**, *15*, 4844-4858.

[23] Thurn, K.T.; Arora, H.; Paunesku, T.; Wu, A.; Brown, E. M.; Doty, C.; Kremer, J.; Woloschak, G. Endocytosis of titanium dioxide nanoparticles in prostate cancer PC-3M cells. *Nanomedicine* **2011**, *7*, 123-130.

[24] Huang, K.; Chen, L.; Deng, J.; Xiong, J. Enhanced Visible-Light Photocatalytic Performance of Nanosized Anatase TiO_2 Doped with CdS Quantum Dots for Cancer-Cell Treatment. *Journal of Nanomaterials* **2012**, *2012*, 1-12.

[25] Mallik, A.; Bryan, S.; Puukila, S.; Chen, A.; Khaper, N. Efficacy of Pt-modified $TiO_{(2)}$ nanoparticles in cardiac cells. *Experimental and clinical cardiology* **2011**, *16*, 6-10.

[26] Nolan, M. Electronic coupling in iron oxide-modified TiO_2 leads to a reduced band gap and charge separation for visible light active photocatalysis. *Physical chemistry chemical physics: PCCP* **2011**, *13*, 18194-18199.

[27] Jokerst, J. V.; Lobovkina, T.; Zare, R. N.; Gambhir, S. S. Nanoparticle PEGylation for imaging and therapy. *Nanomedicine* **2011**, *6*, 715-728.

[28] Buonsanti, R.; Grillo, V.; Carlino, E.; Giannini, C.; Curri, M. L.; Innocenti, C.; Sangregorio, C.; Achterhold, K.; Parak, F. G.; Agostiano, A.; Cozzoli, P. D. Seeded growth of asymmetric binary nanocrystals made of a semiconductor TiO_2 rodlike section and a magnetic gamma-Fe_2O_3 spherical domain. *Journal of the American Chemical Society* **2006**, *128*, 16953-16970.

[29] Sarkar, R.; Ghosh, M.; Pal, S. K. Ultrafast relaxation dynamics of a biologically relevant probe dansyl at the micellar surface. *Journal of photochemistry and photobiology B, Biology* **2005**, *78*, 93-98.

[30] Holmes-Farley, S. R.; Whitesides, G. M. Fluorescence properties of dansyl groups covalently bonded to the surface of oxidatively functionalized low-density polyethylene film. *Langmuir* **1986**, *2*, 266-281.

[31] Karabacak, M.; Cinar, M.; Kurt, M.; Poiyamozhi, A.; Sundaraganesan, N. The spectroscopic (FT-IR, FT-Raman, UV and NMR) first order hyperpolarizability and HOMO-LUMO analysis of dansyl chloride. *Spectrochimica acta Part A, Molecular and biomolecular spectroscopy* **2014**, *117*, 234-244.

[32] Capasso, D.; de Paola, I.; Liguoro, A.; Del Gatto, A.; Di Gaetano, S.; Guarnieri, D.; Saviano, M.; Zaccaro, L. RGDechi-hCit: alphavbeta3 selective pro-apoptotic peptide as potential carrier for drug delivery into melanoma metastatic cells. *PLoS One* **2014**, *9*, e106441.

[33] Graf, N.; Bielenberg, D. R.; Kolishetti, N.; Muus, C.; Banyard, J.; Farokhzad, O. C.; Lippard, S. J. alpha(V)beta(3) integrin-targeted PLGA-PEG nanoparticles for enhanced anti-tumor efficacy of a Pt(IV) prodrug. *ACS Nano* **2012**, *6*, 4530-4539.

[34] Castel, S.; Pagan, R.; Mitjans, F.; Piulats, J.; Goodman, S.; Jonczyk, A.; Huber, F.; Vilaró, S.; Reina, M. RGD peptides and monoclonal antibodies, antagonists of alpha(v)-integrin, enter the cells by independent endocytic pathways. *Lab Invest.* **2001**, *81*, 1615-26.

[35] Aguzzi, M. S.; Fortugno, P.; Giampietri, C.; Ragone, G.; Capogrossi, M. C.; Facchiano, A. Intracellular targets of RGDS peptide in melanoma cells. Mol Cancer. 2010; 9: 84.